Theor Chem Acc (2011) 130:361–369
DOI 10.1007/s00214-011-0999-4

REGULAR ARTICLE

Self-interaction artifacts on structural features of uranyl monohydroxide from Kohn–Sham calculations

Raghunathan Ramakrishnan · Alexei V. Matveev · Sven Krüger · Notker Rösch

Received: 7 April 2011 / Accepted: 9 July 2011 / Published online: 29 July 2011

Abstract Invoking a DFT + U approach, we explored self-interaction artifacts in results from Kohn–Sham (KS) density functional calculations on the geometry and the vibrational frequencies of uranyl monohydroxide and the corresponding tetra-aqua complex. Exchange–correlation functionals based on the local density approximation (LDA) and the generalized-gradient approximation (GGA) predict equilibrium geometries for $[UO_2(OH)]^+$ that deviate from the results of hybrid DFT calculations and high-level wavefunction-based methods such as CCSD(T). LDA + U and GGA + U functionals with corrections for the insufficient localization of the U 5*f* shell yield better agreement, in particular for the angle U-O_h-H. At the LDA level, a linear coordination of the OH ligand results; with the +U correction, the angle U-O_h-H is reduced by $\sim 35°$, in good agreement with CCSD(T) results. At the GGA level, the bending angle is changed by $\sim 20°$. This relatively strong self-interaction artifact is traced back to a spurious π interaction between U 5*f* and O(*p*) orbitals which is less pronounced in the presence of further (aqua) ligands.

Keywords Self-interaction · Density functional theory · DFT + U · Uranyl monohydroxide

Dedicated to Professor Shigeru Nagase on the occasion of his 65th birthday and published as part of the Nagase Festschrift Issue.

Electronic supplementary material The online version of this article (doi:10.1007/s00214-011-0999-4) contains supplementary material, which is available to authorized users.

R. Ramakrishnan · A. V. Matveev · S. Krüger · N. Rösch (✉)
Department Chemie and Catalysis Research Center,
Technische Universität München, 85747 Garching, Germany
e-mail: roesch@mytum.de

1 Introduction

Recently we showed [1, 2] that commonly used exchange–correlation functionals can result in self-interaction artifacts when applied to lanthanide and actinide molecules, and we used a DFT + U approach [3] as a simple and convenient tool for tracing such artifacts to the insufficient description of the metal *f* shells. Here we extend these studies to uranyl monohydroxide $[UO_2(OH)]^+$ and the corresponding tetra-aqua complex by calculating geometries and vibrational modes, and analyzing the electronic structure of these complexes.

The uranyl dication UO_2^{2+} is a stable linear molecule. Participation of both 5*f* and 6*d* orbitals in the uranyl bonds is responsible for the stability and the linearity of the uranyl framework [4]. In coordination complexes of uranyl, the ligands are predominantly confined to the equatorial plane perpendicular to the uranyl moiety [5]. In aqueous solution, the uranyl ion is usually coordinated by aqua ligands. In dilute solutions, already at acidic pH, solvated $[UO_2(OH)]^+$ appears as a hydrolysis product of uranyl [6]. $[UO_2(OH)]^+$ has been observed in the gas phase as product of O_2 oxidation of $[UO(OH)]^+$ both in an ion trap-secondary ion mass spectrometric experiment [7] and in an electrospray ionization (ESI) experiment of aqueous uranyl solution [8]. Computational models predicted that uranyl (VI) complexes of the type UO_2^{2+}-X with the equatorial ligands X = H_2O [9], H^- [10], F^- [11], OH^- [10, 12] or O^{2-} [13, 14] feature a bent uranyl moiety, with the deviation of linearity increasing with the bond strength of the ligands.

For a strong ligand such as hydroxyl, it is of interest to study the bond between the U atom and the equatorial ligand and the possibility of a 5*f* contribution to this bond. Uranyl monohydroxide species, in the gas phase and as

hydrated complex, have been the subject of several theoretical studies [9, 10, 15–17]. In these works, detailed geometry parameters such as bond angles were not discussed. In experimental investigations [7, 8] of $[UO_2(OH)]^+$ in the gas phase, structural features of the molecule were helpful for deducing the kinetics of water adduct reactions and collision-induced dissociation pathways of water and alcohol adduct complexes.

For $[UO_2(OH)]^+$, our density functional calculations employing local density (LDA) or gradient-corrected (GGA) exchange–correlation (XC) functionals yielded geometry parameters that deviate notably from CCSD(T) results. For this closed-shell species, where static correlation effects are absent, CCSD(T) predictions should provide a fairly accurate reference. To analyze the geometric deviations of Kohn–Sham (KS) calculations on $[UO_2(OH)]^+$, we used the DFT + U methodology [3], as recently implemented by us for the first time for molecules [1, 2].

The self-interaction error of common XC functionals artificially stabilizes delocalized states, whereas solvent effects stabilize localized states [18]. Thus, one can expect relatively large self-interaction artifacts for species in the gas phase and a reduction of these effects in the presence of aqua ligands due to the preference for localized states in solution. To confirm this expectation, we also inspected the hydrated complex $[UO_2(OH)(H_2O)_4]^+$.

In the following, we first describe the methods and models used in this study. Then we discuss our results for the geometry and the vibrational frequencies of uranyl monohydroxide as well as the bonding of the hydroxide ligand in this complex with regard to self-interaction-related artifacts. Finally, we analyze the geometrical features of the hydrated congener.

2 Methods and models

We carried out scalar relativistic all-electron Douglas-Kroll-Hess (AE-DKH) calculations [19–21] with the linear combination of Gaussian-type orbitals fitting-functions density functional (LCGTO-FF-DF) method [22] as implemented in the code ParaGauss [22–24]. We employed the local density functional in the parameterization of Vosko, Wilk, and Nusair (VWN) [25] and the gradient-corrected PBE functional [26]. We refer to the corresponding DFT + U calculations with the designators VWN + U and PBE + U. In our AE-DKH-DFT and AE-DKH-DFT + U calculations using the program ParaGauss [23], we used the same orbital basis sets for U, O and H atoms along with polarization functions, charge-fit auxiliary basis sets and grid settings for numerical integration of XC contributions as in our previous study [2]. All geometry optimizations for the molecule $[UO_2(OH)]^+$ were performed by enforcing C_s point group symmetry while we did not apply any symmetry restrictions for the hydrated complex $[UO_2(OH)(H_2O)_4]^+$. Vibrational frequencies were calculated by estimating the elements of the Hessian as finite differences of displacement gradients that had been determined analytically.

The Hubbard-like DFT + U correction term to the total energy [3] in a simple, rotationally invariant form [27] depends on a single on-site effective Coulomb repulsion parameter U_{eff}. The DFT + U penalty functional provides an approximate, easily tunable energy correction of the self-interaction error for partially occupied quasi-atomic shells [28], which is applied here to the 5*f* shell of uranium [2]. The particular functional which we employed in the present work has been classified as the fully localized limit form of the DFT + U correction term [29]. In the present work, we employed the same range of U_{eff} parameters, i.e., 0.0–2.0 eV, as in our previous study [2], which we found reliable for the uranyl molecule. This range was chosen to reproduce approximately the successive ionization potentials of the molecules UO and UO_2 [2].

To generate an accurate reference, free of self-interaction artifacts, we employed CCSD(T) results for $[UO_2(OH)]^+$ which were determined with the quantum chemistry package MOLPRO-2008.1 [30] using for the U atom an atomic natural orbital (ANO) valence basis set (14*s*, 13*p*, 10*d*, 8*f*, 6*g*) → [6*s*, 6*p*, 5*d*, 4*f*, 3*g*], contracted in generalized fashion [31], and the relativistic effective core potential (RECP) ECP60MWB [32]; the aug-cc-pVTZ basis sets were utilized for H [33] and O [34] atoms. In addition, we carried out RI-DFT B3LYP, RI-DFT PBE0 and MP2 calculations with the program Turbomole-6.1 [35], employing the same basis sets for O, H, and U atoms (and the RECP for U) as in the CCSD(T) calculation, but the def-TZVP segmented contracted valence basis set (14*s*, 13*p*, 10*d*, 8*f*, 1*g*) → [10*s*, 9*p*, 5*d*, 4*f*, 1*g*] [36] for U and the m3 quadrature grid. The segmented contracted basis set used for the U atom in the Turbomole calculations is slightly larger than the generalized contracted basis set used with the program MOLPRO; both basis sets have been shown to give very similar results for atomic and molecular systems [36].

In the ParaGauss DFT and DFT + U calculations and in the Turbomole B3LYP, PBE0, and MP2 calculations, the total energies were converged to 10^{-8} hartree and the geometries were optimized until the Cartesian gradient norms were less than 10^{-5} hartree/bohr. In the MOLPRO CCSD(T) calculation, the convergence criteria enforced on the one-particle density, Hartree–Fock energies, CCSD(T) energies, and Cartesian gradient norms were 10^{-8}, 10^{-10} hartree, 10^{-8} hartree, and 10^{-3} hartree/bohr, respectively.

3 Results and discussion

3.1 Geometry

Table 1 summarizes the geometry parameters of uranyl monohydroxide in the gas phase as calculated at different theoretical levels of theory such as PBE, PBE + U, VWN [10], VWN + U, PW91 [10], B3LYP [10], PBE0, MP2 [17], and CCSD(T). As no experimental geometry is available for the molecule $[UO_2(OH)]^+$ in the gas phase, the equilibrium geometry calculated by the CCSD(T) method is chosen as a reliable reference. At the VWN level, we estimated the incremental changes of various basis sets and of the RECP approximation on the CCSD(T) results. As a result, we derived the following reference results obtained from the CCSD(T) calculations: U-O_t = 174.1 pm, U-O_h = 201.8 pm (both with an uncertainty of ±0.5 pm), and O_t-U-O_t = 170.7°, U-O_h-H = 148.1° (both with an uncertainty of ±0.5°; see Table 1 and Table S1 of Supplementary Material).

To inspect the effect of self-interaction, we carried out all-electron VWN and PBE density functional calculations as well as the corresponding DFT + U calculations for U_{eff} = 1 and 2 eV. Bond lengths as obtained with the VWN functional show small deviations from the CCSD(T)-derived reference. The uranyl bond U-O_t = 174.9 pm overestimates the reference by 0.8 pm, while U-O_h = 199.1 pm underestimates the reference by 2.7 pm. The uranyl angle O_t-U-O_t = 168° (Fig. 1) is only slightly smaller than the reference value, 171°. As the most remarkable difference between CCSD(T) and VWN calculations, one notes the U-O_h-H angle which is 148° for CCSD(T), where the VWN calculations yield a linear ligand configuration (180°). This remarkable failure has been observed earlier in a VWN-RECP calculation [10] and is also reproduced in our VWN-RECP calculations (Table S1). DFT + U results obtained with the VWN functional yield shorter uranyl bonds and a longer U-O_h bond; changes increase with U_{eff} (Table 1). The structure parameters calculated for U_{eff} = 2 eV, U-O_t = 174.0 pm and U-O_h = 201.2 pm agree with the reference within the uncertainties due to the basis sets (see above and Table 1). The uranyl angle O_t-U-O_t increases with increasing U_{eff} from 168° to 175°, finally slightly overestimating the reference of 171°. The most prominent effect of the DFT + U method is a strong decrease of the U-O_h-H angle, from 180° for U_{eff} = 0 eV to 145° for U_{eff} = 2 eV, which agrees very well with the CCSD(T) reference of 148° (Table 1). Figure 2 shows scans of the potential energy at the VWN + U level when the angle U-O_h-H is varied for different values of U_{eff}. For U_{eff} = 0 eV, a wide minimum for U-O_h-H = 180° results. Increasing U_{eff} leads to a distortion that resembles a second-order Jahn–Teller effect [37] with a minimum energy at reduced angles U-O_h-H. Overall, the

Table 1 Geometry parameters of $[UO_2(OH)]^+$ calculated at the PBE and PBE + U levels along with results from other computational methods: average bond length U-O_t, bond length U-O_h, bond angle O_t-U-O_t, O_t-U-O_h, and U-O_h-H

Method	U_{eff}	U-O_t	U-O_h	O_t-U-O_t	U-O_h-H
AE-DKH-VWN		174.9	199.1	168.3	180.0
AE-DKH-VWN + U	1.0	174.4	200.1	172.2	153.7
AE-DKH-VWN + U	2.0	174.0	201.2	174.9	144.5
AE-DKH-PBE		176.5	202.1	166.7	158.8
AE-DKH-PBE + U	1.0	176.1	203.1	171.2	145.6
AE-DKH-PBE + U	2.0	175.6	204.2	174.1	138.6
VWN/RECP[a]		174.7	198.5	167.6	180.0
ZORA-PW91[a]		176.1	201.9	167.9	151.8
B3LYP/RECP		174.2	201.4	167.9	154.2
B3LYP/RECP[a]		175.1	199.9	167.2	
PBE0/RECP		172.3	200.0	170.0	149.4
MP2/RECP		177.7	200.3	171.8	140.0
MP2/RECP[b]		176.7			
CCSD(T)/RECP		173.6	201.3	170.7	148.1
CCSD(T) corr.[c]		174.1	201.8	170.7	148.1

Also given is the Hubbard parameter U_{eff} (eV) for the U 5*f* shell. Distances in pm, angles in degree

Symmetry constraints of point group C_s applied

[a] Ref. [10]

[b] Ref. [17]

[c] Corrected for RECP effects, see Supplementary Material, Table S1. Uncertainty of bond lengths ± 0.5 pm, and of angles ± 0.5°

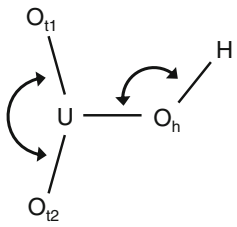

Fig. 1 Sketch of the uranyl monohydroxide complex with atomic labels used

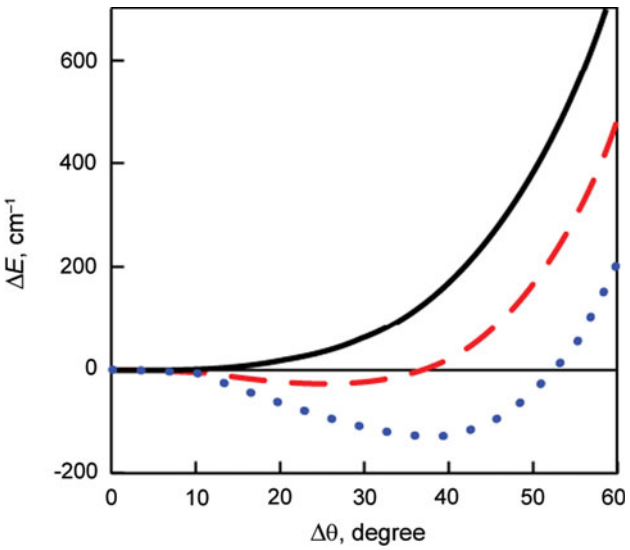

Fig. 2 Potential energy profiles of $[UO_2(OH)]^+$ along the U-O_h-H bending mode from AE-DKH-VWN (*solid line*) and AE-DKH-VWN + U calculations (*red dashed line* $U_{eff} = 1.0$ eV, *blue dotted line* $U_{eff} = 2.0$ eV). For various angles $\Delta\theta$ of deviation from linearity (180°) of the U-O_h-H fragment, relative energies ΔE (cm^{-1}) of $[UO_2(OH)]^+$ are plotted. The energies were obtained by constrained geometry optimizations of $[UO_2(OH)]^+$ by fixing the angle of the U-O_h-H fragment at various values

DFT + U approach leads to a notable improvement in the VWN results.

Comparison of PBE and DFT + U PBE results reveals the same trends when varying U_{eff} as obtained for the VWN calculations (Table 1). The bond U-O_t = 176.5 pm at the PBE level overestimates the reference, 174.1 pm; the reduction by 0.9 pm due to self-interaction correction ($U_{eff} = 2$ eV) only partially accounts for this deviation. The bond U-O_h = 202.1 pm is already overestimated at the PBE level and is elongated even further in the DFT + U calculations, to 204.2 pm ($U_{eff} = 2$ eV). Both changes of the bond lengths due to the self-interaction correction, −0.9 pm for U-O_t and 2.1 pm for U-O_h, agree with the corresponding corrections at the VWN level (Table 1). Also the uranyl angle O_t-U-O_t increases with increasing U_{eff} from 167° (0 eV) to 174° (2 eV), slightly overestimating the CCSD(T) result of 171°. In contrast to the VWN results, the PBE calculations yield a bent OH ligand structure with an angle U-O_h-H of 159°, which decreases to 139° for $U_{eff} = 2$ eV. Thus, PBE slightly overestimates that angle and the DFT + U corrections result in a comparable underestimation of ~10° (Table 1). Overall, comparison of VWN and PBE results reveals the often observed overestimation of bond lengths of heavy element compounds for GGA compared to LDA [38, 39]. Similar results as obtained here with the PBE functional have earlier been calculated with the PW91 GGA functional, applying the all-electron ZORA scalar relativistic approach (Table 1) [10].

Our B3LYP/RECP calculation yields a structure that agrees well with the CCSD(T) reference. The uranyl bond calculated as 174.2 pm as well as the U-O_h bond of 201.4 pm very well match the CCSD(T) values of 173.6 and 201.3 pm, respectively. Also the angular parameters O_t-U-O_t = 168° and U-O_h-H = 154° agree satisfactorily with the reference, deviating at most by 6° (Table 1). A previous B3LYP calculation furnished slightly worse bond distances, U-O_t = 175.1 pm and U-O_h = 199.9 pm. Also, the bond distances determined with the PBE0 hybrid functional and a small core RECP, U-O_t = 172.3 pm and U-O_h = 200.0 pm deviate slightly more from the reference than our B3LYP/RECP results. On the other hand, the PBE0 calculation yields rather accurate angles, O_t-U-O_t = 170° and U-O_h-H = 149°, which agree within 2° with the reference values. Hybrid functionals obviously provide more accurate results than LDA and GGA calculations. This improved performance can be rationalized in part by the inclusion of an admixture of "exact" exchange in these functionals which reduces self-interaction artifacts. Interestingly, MP2 calculations, which are free of any self-interaction error, yield rather long U-O_t bonds for $[UO_2(OH)]^+$, 177.7 pm (this work), and 176.7 pm [17], comparable to GGA results (Table 1). On the other hand, the bond U-O_h = 200.3 pm, as well as the angles O_t-U-O_t = 172° and U-O_h-H = 140°, obtained with the MP2 approach, agrees well with the CCSD(T) reference. Thus, the relatively long bond lengths obtained in GGA and MP2 calculations are not the result of a remaining unphysical self-interaction, but have to be ascribed to an insufficient representation of correlation.

As essential effects of self-interaction, our DFT + U results show a weakening and elongation of the uranyl bond and, as a consequence of bonding competition at the uranium center, a contraction of the U-O_h ligand bond. Due to the presence of the hydroxyl ligand, uranyl is slightly bent (Table 1). As we showed earlier [2], this effect decreases with increasing U_{eff}, in line with an increasing frequency of the corresponding bending vibrational mode. The strong effect of U_{eff} on the angle U-O_h-H is an indirect effect due to the bending of uranyl. Optimizations of $[UO_2(OH)]^+$ with a fixed linear uranyl moiety carried out at the PBE and PBE + U levels yield much smaller effects

Table 2 Harmonic vibrational frequencies ω (cm^{-1}) of $[UO_2(OH)]^+$ calculated at various DFT and DFT + U levels along with results from other methods

Method	U_{eff}	ω_1	ω_2	ω_3	ω_4	ω_5	ω_6	ω_7	ω_8	ω_9
AE-DKH-VWN[a]		3,669	1,010	928	694	513	269	227	95	140
AE-DKH-VWN + U[b]	1.0	3,674	1,026	936	686	530	332	219	182	170
AE-DKH-VWN + U[c]	2.0	3,677	1,039	944	648	542	381	234	217	197
AE-DKH-PBE[d]		3,680	976	895	660	500	311	200	117	145
AE-DKH-PBE + U[e]	1.0	3,680	989	901	650	510	374	213	204	170
AE-DKH-PBE + U[e]	2.0	3,686	1,003	909	643	538	439	240	213	195
B3LYP/RECP		3,769	1,026	946	672	515	321	207	168	165
B3LYP/RECP[f]			1,025	946	679					
PBE0/RECP		3,823	1,068	990	691	533	350	216	193	179
MP2/RECP		3,770	973	878	701	587	400	219	90	164
MP2/RECP[g]			969	884						
CCSD(T)/RECP		3,810	1,022	944	683	553	340	210	185	168
Exp.[h]				849						

Also given is the Hubbard parameter U_{eff} (eV) for the U 5*f* shell as well as available experimental data

Main assignment: ω_1 (a′)—O_h-H stretching, ω_2 (a′)—U-O_t asymmetric stretching, ω_3 (a′)—U-O_t symmetric stretching, ω_4 (a′)—U-O_h stretching, ω_5 (a″)—O_h-H torsion, ω_6 (a′)—U-O_h-H bending, ω_7 (a′)—O_t-U-O_t scissoring, ω_8 (a′)—O_t-U-O_t rocking mixed with O_t-U-O_h bending modes, ω_9 (a″)—O_t-U-O_t wagging. Deviations for the three low-frequency modes ω_6 to ω_8 are specified explicitly. For kinetic energy distribution data, see Table S4. For the designation of the atoms, see Fig. 1

Symmetry constraints of point group C_s applied

[a] ω_6—O_t-U-O_h bending with a contribution from U-O_h-H bending, ω_8—O_t-U-O_h in-plane bending

[b] ω_7—admixture of O_{t2}-U-O_h bending

[c] ω_6—admixture of O_t-U-O_t rocking, ω_7—admixture of U-O_h-H bending, ω_8—admixture of U-O_h-H bending

[d] ω_6—admixture of O_{t1}-U-O_h bending, ω_7—admixture of U-O_h-H bending, ω_8—O_{t1}-U-O_h in-plane bending with admixture of U-O_h-H bending

[e] ω_8—O_{t2}-U-O_h in-plane bending

[f] Ref. [10]

[g] Ref. [17]

[h] Aqueous phase, Ref. [6]

(Table S3). In unconstrained optimizations, U-O_h-H decreases by 20° when U_{eff} increases from 0 to 2 eV, while for a fixed linear uranyl moiety, this angle decreases by 6° for the same variation of U_{eff}. This finding is of special interest as it shows that indirect effects of self-interaction artifacts for geometry parameters may be sizeable for soft degrees of freedom. Fixing the uranyl bond angle at 180° affects the changes in bond length only marginally when U_{eff} is varied (Table S3).

3.2 Vibrational frequencies

Next we will discuss vibrational frequencies of normal modes of $[UO_2(OH)]^+$ as calculated by various methods (Table 2) to support the interpretation of self-interaction effects on geometry parameters. As we showed on the example of VWN calculations, the RECP approximation hardly affects the calculated vibrational frequencies (Table S2).

In order of decreasing frequency values, the vibrational modes qualitatively represent the O–H stretching mode ω_1 at $\sim$3,700 cm^{-1}, the asymmetric and symmetric stretching modes ω_2 and ω_3 of uranyl at about 1,000 and 950 cm^{-1}, respectively, the U-O_h stretching and torsion modes ω_4 and ω_5 at about 650 and 550 cm^{-1}, respectively, followed by four low-frequency bending modes which are less well defined in character and tend to mix among each other when different methods or U_{eff} values are compared.

At the LDA and GGA levels, the O–H stretching frequency is underestimated by more than 100 cm^{-1} compared to the CCSD(T) reference (Table 2). This goes along with corresponding differences in the O–H bond length, which amounts to $\sim$97 pm for CCSD(T) and 98 pm in LDA and GGA calculations. These deviations of the O–H bond length and the corresponding frequencies cannot be attributed to U 5*f*-related self-interaction artifacts, as the DFT + U approach yields only a marginally larger frequency, by 6–8 cm^{-1} (Table 2). Results of B3LYP and MP2 calculations agree much better with the CCSD(T) reference; therefore, correlation effects may be responsible for these deviations.

In agreement with the slight overestimation of the uranyl bond length by the VWN approach compared to the CCSD(T) reference, the corresponding stretching mode frequencies ω_2 and ω_3 are calculated slightly too low, by 12 cm^{-1} for the asymmetric mode and by 16 cm^{-1} for the symmetric mode. In line with the decrease in the uranyl bond lengths for VWN + U results, the corresponding frequencies are calculated larger, by 29 cm^{-1} for ω_2 and 16 cm^{-1} for ω_3 with $U_{eff} = 2$ eV. Thus, while ω_2 with 1,039 cm^{-1} overestimates the reference by 17 cm^{-1}, ω_3 by chance fits the reference perfectly. For the PBE approach, the same trends as for the VWN results are obtained. In agreement with the overestimation of bond lengths by the GGA approach (Table 1), uranyl stretching frequencies are calculated too low even with the PBE + U method (Table 2), by 19 cm^{-1} for ω_2 and 25 cm^{-1} for ω_3 for $U_{eff} = 2$ eV. The U-O_h stretching mode ω_4, calculated at 694 cm^{-1} with the VWN approach, is slightly higher than the CCSD(T) reference, 683 cm^{-1}, and decreases with growing U_{eff} to 648 cm^{-1} for $U_{eff} = 2$ eV in the VWN + U calculations. This trend is in line with the finding that the bond U-O_h is calculated to increase with U_{eff} (Table 2). As for ω_2, the effect of self-interaction correction is overestimated for $U_{eff} = 2$ eV, but the result of 686 cm^{-1} for $U_{eff} = 1$ eV agrees with the CCSD(T) reference of 683 cm^{-1}. In PBE calculations, ω_4 is again underestimated, by 23 cm^{-1}. This difference to the CCSD(T) reference increases with increasing U_{eff} and reflects the overestimation of bond length by the GGA approach.

The last larger frequency is the U-O_h-H torsion mode ω_5, calculated at 513 cm^{-1} at the VWN level, well below the reference of 553 cm^{-1} (Table 2). With the VWN + U approach ($U_{eff} = 2$ eV), one obtains a larger frequency, 542 cm^{-1}, in fair agreement with the CCSD(T) calculation. A similar trend as for VWN is obtained at the PBE level with increasing U_{eff}, except that the GGA frequencies are lower, as usual (Table 2). The slight strengthening of this mode in the DFT + U calculations may be due to a larger spurious uranium-ligand in-plane π interaction that competes with the O–H bonding.

The four lowest vibrational modes all show an increasing trend with growing U_{eff}; for VWN + U and $U_{eff} = 1$ eV, the results agree well with CCSD(T) reference (Table 2), whereas PBE + U values are on average a little worse. Two of these modes, ω_6 and ω_8, mainly represent the in-plane U-O_h-H bending mode and the uranyl rocking mode, respectively. They increase strongly with U_{eff}, by more than 100 cm^{-1} on going from 1 to 2 eV. This finding agrees with our earlier calculations for the bending mode of uranyl which also yielded a frequency that strongly increases with U_{eff} [2]. These two modes tend to mix with the uranyl scissoring motion ω_7 (Table 2). The uranyl out-of-plane wagging mode ω_9 is less sensitive to U_{eff} in VWN and PBE calculations, with changes of about 50 cm^{-1} on going from 0 to 2 eV.

3.3 Electronic structure

To inspect the effect of the correction term of the DFT + U method on the electronic structure of $[UO_2(OH)]^+$, we performed a Mulliken population analysis. Table 3 summarizes the Mulliken gross atomic populations of six valence molecular orbitals (MOs) of $[UO_2(OH)]^+$. This set includes all MOs with sizeable U 5*f* contributions as well as MOs with notable $O_h(p)$ contributions of the oxygen center of the hydroxyl ligand; the latter MOs contribute to the uranyl-ligand bond. As the essential features of these valence orbitals are very similar at the VWN and PBE levels, we discuss the VWN results only for $U_{eff} = 0$ and 2.0 eV. The corresponding PBE and PBE + U results are provided as Supplementary Material, see Table S5.

Table 3 Population analysis of valence molecular orbitals of $[UO_2(OH)]^+$ with notable U 5*f* and ligand O(*p*) contributions: energies ε_i (eV) and Mulliken atomic gross populations (as percentage) from AE-DKH-VWN and AE-DKH-VWN + U calculations

Type	MO	VWN					VWN + U[a]				
		ε_i	U *f*	O_{t1} *p*	O_{t2} *p*	O_h *p*	ε_i	U *f*	O_{t1} *p*	O_{t2} *p*	O_h *p*
a′	41	−12.94	31	12	12	38	−12.99	17	7	9	59
	40	−14.68	17	34	33	4	−15.09	25	50	4	10
	39	−14.68	34	14	14	31	−14.71	35	6	35	10
	36[b]	−18.23	7	2	2	53	−17.84	7	5	2	52
a″	17	−14.44	10	5	5	71	−14.04	6	0	1	81
	16	−15.18	26	28	28	12	−15.39	29	31	34	1

Symmetry constraints of point group C_s applied. For atomic labels see Fig. 1

[a] $U_{eff} = 2.0$ eV for the 5*f* shell of U

[b] Both in the VWN and VWN + U calculations, this MO has a 15% H(1*s*) contribution, which is not listed. This MO is of $O_h(2p)$–H(1*s*) σ character

First of all, the effect of DFT + U for $U_{eff} = 2.0$ eV on the electronic structure is relatively small, despite the marked effects on the geometry discussed above. The U 5*f* population decreases only slightly from 2.9 *e* at $U_{eff} = 0$ eV to 2.8 *e* at $U_{eff} = 2.0$ eV. The lowest lying orbital of the VWN valence electronic structure listed in Table 3, MO 36 a′ at −18.2 eV, with about 50% of $O_h(p)$ character and 15% of H(*s*) character, represents the ligand O–H bond with very small admixtures from the uranyl moiety. Without changing its character, this orbital is destablized by ∼0.4 eV in the DFT + U approach. The next lowest MO 16 a″ at −15.2 eV is essentially an out-of-plane uranyl π orbital which is also of π character with respect to the O–H bond; it shows a small $O_h(p)$ bonding admixture (Table 3). The localization of the U 5*f* orbitals decreases the admixture of $O_h(p)$ character from 12 to 1% and leads to a slight stabilization of this orbital by 0.2 eV which reflects the strengthening of the uranyl bond. The corresponding U-O_h π antibonding orbital, 17 a″, which is of weak uranyl π antibonding character, correspondingly is destablized by the localization of the U 5*f* orbitals. While in the VWN calculation, it shows 10% U *f* contribution and 71% $O_h(p)$ character, the U *f* contribution decreases to 6% and the $O_h(p)$ character increases to 81% in the VWN + U calculation, leading to a rather pure lone pair orbital of the ligand. Thus, at the VWN + U level, the interaction between the U *f* out-of-plane uranyl π orbital and the out-of-plane ligand *p* lone pair orbital decreases. This contributes to a stabilization of the uranyl bond and destabilization of the uranium ligand bond, as confirmed by the geometry results. The three higher lying MOs of a′ character, 39 a′, 40 a′, and the HOMO 41 a′, all exhibit considerable U 5*f* contributions. MO 39 a′ is of uranyl σ character and at the VWN level shows a sizeable admixture of $O_h(p)$, ∼30%, of U-O_h in-plane π character. In the VWN + U electronic structure, this U-O_h π admixture decreased to about one-third as consequence of the localization of the U 5*f* orbitals, concomitant with a marginal stabilization of the 39a′ MO. As U-O_h in-plane π bonding favors a linear coordination of the OH ligand, the loss of this orbital mixing facilitates the bending of the OH ligand, as the corresponding O_h (*p*) character can contribute to the O–H bond. MO 40 a′ is predominantly of uranyl in-plane π-bonding character. Its U 5*f* contribution increases, as these atomic orbitals are localized, from 17 to 25%; the resulting stabilization of this orbital by 0.4 eV contributes to the strengthening of the uranyl bond. In the VWN calculation with the linear coordination of the OH ligand, the HOMO 41 a′ is of uranyl in-plane δ character with a strong U *f* contribution of ∼30%; this MO features a sizeable π bonding interaction with the OH ligand (Fig. 3) which stabilizes its linear coordination. Correction for self-interaction artifacts by the VWN + U method lowers the U *f* contribution to about one-half and leads to a corresponding increase of the $O_h(p)$ character. As a result, the HOMO acquires more the character of an $O_h(p)$ lone pair with a weak σ overlap to the U 5*f* orbitals.

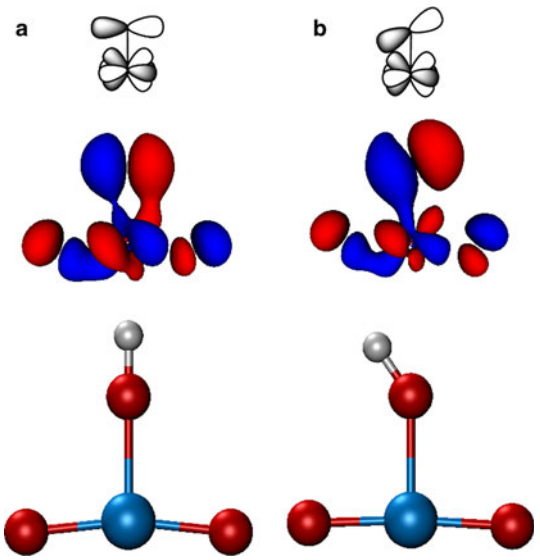

Fig. 3 Equilibrium geometry and structure of the 41 a′ HOMO orbital of uranyl monohydroxide: **a** AE-DKH-VWN, **b** AE-DKH-VWN + U ($U_{eff} = 2.0$ eV). The interaction between the uranyl dication and the hydroxyl ligand in $[UO_2(OH)]^+$ changes its character from short-range π to "long-range" weak pseudo-σ interaction. In the simplified schematic representation (*top*) of the orbital interaction, the uranyl σ-like contribution is omitted for clarity

In summary, the bending of the OH ligand as a result of the localization of the U 5*f* orbitals in the DFT + U approach can be traced back to a reduction of the in-plane π-donation of the ligand, which is artificially facilitated when the U 5*f* orbitals are delocalized at the LDA and GGA levels.

3.4 The aqua complex

Finally, we examine the effect of a complete ligand shell on the self-interaction artifacts of $[UO_2(OH)]^+$ for the example of the tetra aqua complex $[UO_2(OH)(H_2O)_4]^+$. In this complex, the uranyl moiety features coordination number 5, as is often preferred for uranyl [40], due to four additional aqua ligands. Table 4 summarizes parameters of the equilibrium geometry of $[UO_2(OH)(H_2O)_4]^+$ from AE-DKH-PBE and AE-DKH-PBE + U calculations, along with results obtained with other methods such as B3LYP [12, 15], ZORA-PBE [16], ZORA-BP86 [16], MP2 [17], and CCSD [17].

Our AE-DKH-PBE results show the expected effects of coordination by aqua ligand on the structure of the UO_2OH moiety. The uranyl bond is elongated by ∼4 to 180 pm and the U-O_h bond increases from 202 to 212 pm due to bond

Table 4 Geometry parameters of $[UO_2(OH)(H_2O)_4]^+$ calculated at the PBE and PBE + U levels along with results from other methods

Method	U_{eff}	U-O_t	U-O_w	U-O_h	O_t-U-O_t	U-O_h-H
AE-DKH-PBE		180.1	257	212.3	169.3	133.4
AE-DKH-PBE + U	1.0	179.5	258	212.8	172.4	129.1
AE-DKH-PBE + U	2.0	178.9	259	214.3	174.6	125.9
ZORA-PBE[a]		179.7	260	211.3		
ZORA-BP86[a]		180.0	259	211.6		
B3LYP/RECP		177.2	259	210.2	173.5	137.5
B3LYP/RECP[b]		178.3		216.2		
B3LYP/RECP[c]		178.6	258	215.5	166.7	
MP2/RECP[d]		177.6	255–260	213.2		
CCSD/RECP[d]		175.1	254–259	214.4		

Average bond length U-O_t, bond lengths U-O_w and U-O_h, bond angles O_t-U-O_t and U-O_h-H, bond angle. Also given is the Hubbard parameter U_{eff} (eV) for the U 5*f* shell. Distances in pm, angles in degree

Without symmetry constraints

[a] Ref. [16]

[b] Ref. [15]

[c] Ref. [12]

[d] Ref. [17]

competition with the aqua ligands. Changing by $\sim 3°$, the uranyl angle O_t-U-O_t is only weakly affected. However, the U-O_h-H angle is notably reduced, from 159° to 133°, when uranyl is coordinated by the aqua ligands. This can be rationalized by a decreasing U-O_h π interaction as the U-O_h bond is elongated. As in $[UO_2(OH)]^+$, the PBE calculation also overestimates the U-O_t bonds of $[UO_2(OH)(H_2O)_4]^+$, by 5 pm, compared to the CCSD reference (Table 4). On the other hand, the bond distances U-O_w to the water ligands, 257 pm, and U-O_h, 212 pm, agree fairly well with the corresponding CCSD results, 254–259 and 214 pm, respectively.

Our PBE results for $[UO_2(OH)(H_2O)_4]^+$ compare favorably with those of a ZORA-GGA calculation [16] (Table 4). At the PBE and BP86 levels, also 180 pm was obtained for U-O_t while the U-O_h distances were determined at 211 and 212 pm, respectively, agreeing with the present PBE result within 1 pm. Only the bonds U-O_w to the aqua ligands were obtained up to 3 pm longer in that ZORA-GGA study (Table 4).

The consequences of correcting the self-interaction effects in the PBE + U approach for $[UO_2(OH)(H_2O)_4]^+$ are rather similar to those determined for $[UO_2(OH)]^+$. With increasing U_{eff} the bond length U-O_t decreases, bonds to the ligands increase, the angle O_t-U-O_t increases and the angle U-O_h-H decreases. As for $[UO_2(OH)]^+$, the decrease of U-O_t from 180 to 179 pm ($U_{eff} = 2$ eV) is not sufficient to reach the CCSD result of 175 pm. On the other hand, as indirect result of forming the coordination shell of aqua ligands, U-O_h is no longer overestimated compared to the reference; its elongation to 214 pm ($U_{eff} = 2$ eV) brings it into agreement with the CCSD reference.

Whereas the changes in the bonds of interest due to the PBE + U approach are very similar for $[UO_2(OH)(H_2O)_4]^+$ and $[UO_2(OH)]^+$ (U-O_t: 1 pm; U-O_h: 2 pm), a much weaker effect is calculated on the U-O_h-H angle when the U 5*f* orbitals are more localized. This angle decreases by 8° for $[UO_2(OH)(H_2O)_4]^+$ ($U_{eff} = 2$ eV), whereas this change was 20° for $[UO_2(OH)]^+$. This again is rationalized by a reduction in the U-O_h π interaction as a result of the elongation of the U-O_h bond length after coordination by the aqua ligands.

Similar to our PBE + U results, also the B3LYP/RECP calculations tend to overestimate the U-O_t bond lengths compared to the reference, U-O_t = 175 pm, yielding values of 177–179 pm [12, 15]. Yet, in contrast to our PBE + U result, also the U-O_h bond is slightly overestimated in some B3LYP calculations [12, 15], by 1–2 pm compared to the CCSD result of 214 pm. Interestingly, in the B3LYP calculation performed in the present work, the distance U-O_h, calculated at 210 pm, is considerably below our PBE + U result, 214 pm ($U_{eff} = 2$ eV), but agrees with the CCSD reference. Our B3LYP result for the angle O_t-U-O_t, 174°, nicely agrees with the PBE + U result, 175°, which is by 5° larger than the PBE result. The PBE + U result for the angle U-O_h-H, 126° is considerably smaller than the B3LYP value, 138° (Table 4). In the MP2 calculation [17], the distance U-O_h is also underestimated, by 1 pm compared to CCSD, while all other parameters are in line with B3LYP results [12, 15].

4 Conclusions

We analyzed self-interaction artifacts of DFT LDA and GGA exchange–correlation functionals on the example of the uranyl monohydroxide complex in the gas phase by means of the DFT + U approach. All-electron scalar relativistic Douglas-Kroll-Hess optimizations with the VWN and PBE functionals were carried out and compared to CCSD(T) calculations which are free of self-interaction artifacts. As for uranyl, we determined an elongation of the uranyl bond by ~ 1 pm as a direct effect of self-interaction. The larger contraction of the U-O_h bond, by 2 pm, is interpreted partially as an effect of ligand competition at the U center, but also driven by a spurious bonding π interaction of the ligand to the uranyl moiety. Along with these changes of bond lengths, a stronger bending of uranyl is observed as a self-interaction artifact.

The most prominent effect was found for the angle U-O_h-H. The hydroxyl ligand coordinates in linear fashion at the VWN level, but a bent structure, with U-O_h-H = 140–150°, was obtained in CCSD(T) and DFT + U calculations. This strong structure change was identified as indirect self-interaction artifact, mediated by the artificial bending of uranyl in VWN and PBE calculations. These marked effects on geometry parameters are also reflected in the vibrational frequencies.

Finally, by comparison to the hydrated species $[UO_2(OH)(H_2O)_4]^+$, we showed that indirect effects of self-interaction on geometrical features decrease for fully coordinated uranyl complexes, while the direct effects on bond lengths are still present. As demonstrated by this example, the DFT + U approach provides a useful and efficient method for probing self-interaction artifacts of common LDA and GGA density functional calculations.

Acknowledgments We thank Daniel Opalka for help with the CCSD(T) calculations. RR gratefully acknowledges a fellowship of the Deutsche Akademischer Austauschdienst (DAAD). This work was supported by Bundesministerium für Wirtschaft und Technologie, project No. 02E10186, and Fonds der Chemischen Industrie (Germany).

References

1. Ramakrishnan R, Matveev AV, Rösch N (2009) Chem Phys Lett 468:158
2. Ramakrishnan R, Matveev AV, Rösch N (2011) Comput Theoret Chem 963:337
3. Anisimov VI, Zaanen J, Andersen OK (1991) Phys Rev B 44:943
4. Denning RG (2007) J Phys Chem A 111:4125
5. Fortier S, Hayton YW (2010) Coord Chem Rev 254:197
6. Nguyen-Trung C, Begun GM, Palmer DA (1992) Inorg Chem 31:5280
7. Gresham GL, Gianotto AK, Harrington PD, Cao L, Scott JR, Olson JE, Appelhans AD, Van Stipdonk MJ, Groenewold GS (2003) J Phys Chem A 107:8530
8. Van Stipdonk MJ, Anbalagan V, Chien W, Gresham G, Groenewold G, Hanna D (2003) J Am Soc Mass Spectrom 14:1205
9. Ya V, Antonchenko ES, Kryachko (2008) Theor Chem Acc 120:421
10. Groenewold GS, Gianotto AK, McIlwain ME, Van Stipdonk MJ, Kullman M, Moore DT, Polfer N, Oomens J, Infante I, Visscher L, Siboulet B, de Jong WA (2008) J Phys Chem A 112:508
11. Straka M, Dyall KG, Pyykkö P (2001) Theor Chem Acc 106:393
12. Oda Y, Aoshima A (2002) J Nucl Sci Technol 39:647
13. Shamov GA, Schreckenbach G, Vo TN (2007) Chem Eur J 13:4932
14. Pyykkö P, Li J, Runeberg N (1994) J Phys Chem 98:4809
15. Hay PJ, Martin RL, Schreckenbach G (2000) J Phys Chem A 104:6259
16. Ingram KIM, Häller LJL, Kaltsoyannis N (2006) Dalton Trans 2403
17. Cao Z, Balasubramanian K (2009) J Chem Phys 131:164504
18. Lundberg M, Siegbahn PEM (2005) J Chem Phys 122:224103
19. Häberlen OD, Rösch N (1992) Chem Phys Lett 199:491
20. Rösch N, Krüger S, Mayer M, Nasluzov VA (1996) In: Seminario JM (ed) Recent development and applications of modern density functional theory, theoretical and computational chemistry, vol 4. Elsevier, Amsterdam, p 497
21. Rösch N, Matveev A, Nasluzov VA, Neyman KM, Moskaleva L, Krüger S (2004) In: Schwerdtfeger P (ed) Relativistic electronic structure theory. Part II: applications, theoretical and computational chemistry series, vol 14. Elsevier, Amsterdam, p 656
22. Dunlap BI, Rösch N (1990) Adv Quantum Chem 21:317
23. Rösch N et al. (2006) PARAGAUSS Version 3.1, Technische Universität München
24. Belling Th, Grauschopf Th, Krüger S, Mayer M, Nörtemann F, Staufer M, Zenger C, Rösch N (1999) In: Bungartz H-J, Durst F, Zenger C (eds) High performance scientific and engineering computing, lecture notes in computational science and engineering, vol 8. Springer, Heidelberg, p 439
25. Vosko SH, Wilk L, Nusair M (1980) Can J Phys 58:1200
26. Perdew JP, Burke K, Ernzerhof M (1996) Phys Rev Lett 77:3865
27. Dudarev SL, Botton GA, Savrasov SY, Humphreys CJ, Sutton AP (1998) Phys Rev B 57:1505
28. Solovyev IV, Dederichs PH, Anisimov VI (1994) Phys Rev B 50:16861
29. Ylvisaker ER, Pickett WE, Koepernik K (2009) Phys Rev B 79:035103
30. Werner H-J et al (2008) Molpro, Version 2008.1. A package of Ab initio programs
31. Cao X, Dolg M, Stoll H (2003) J Chem Phys 118:487
32. Dolg M, Stoll H, Preuss H, Pitzer RM (1993) J Phys Chem 97:5852
33. Dunning TH Jr (1989) J Chem Phys 90:1007
34. Kendall RA, Dunning TH Jr, Harrison RJ (1992) J Chem Phys 96:6796
35. Eichkorn K, Treutler O, Oehm H, Häser M, Ahlrichs R (1995) Chem Phys Lett 242:652
36. Cao X, Dolg M (2004) J Mol Struct (Theochem) 673:203
37. Davidson ER, Borden WD (1983) J Phys Chem 87:4783
38. Ziegler T (1991) Chem Rev 91:651
39. Görling SB, Trickey P, Gisdakis N, Rösch (1999) In: Brown J, Hoffmann P (eds) Topics in organometallic chemistry, vol 4. Springer, Heidelberg, p 109
40. Morss LR, Edelstein NM, Fuger J (eds) (2006) The chemistry of the actinide and transactinide elements, vol. 4, 3rd edn. Springer, Dordrecht, Chaps. 22 and 23